Electronic Supplementary Information for

The facilitated magnesium atom adsorption and surface diffusion kinetics via artificial bismuth-based interphases

Honghao Chu[a], Zhonghua Zhang[*,a], Zihao Song[a], Aobing Du[b], Shanmu Dong[b], Guicun Li[*,a] and Guanglei Cui[*,b]

[a]*College of Materials Science and Engineering, Qingdao University of Science and Technology, Qingdao 266042, China*

[b]*Qingdao Industrial Energy Storage Research Institute, Qingdao Institute of Bioenergy and Bioprocess Technology, Chinese Academy of Sciences, Qingdao 266101, P. R. China*

E-mail: guicunli@qust.edu.cn; cuigl@qibebt.ac.cn

This file contains following content:

1. Experimental section

1.1 Experimental Materials

$BiCl_3$ (99.9%), $Bi(CF_3SO_3)_3$ (99.9%) and DME (99.5%, anhydrous) were purchased from Aladdin. Mg foil (100 μm, 99.9%) was provided by North China Magnesium Processing Plant. The APC electrolyte was purchased from DoDoChem, in which the ingredients include anhydrous $AlCl_3$ and phenylmagnesium chloride as solute and THF as solvent.

1.2 Pretreatment of Mg metal anode

Electrode pretreatment is performed in a glovebox filled with Argon. $BiCl_3$ and $Bi(CF_3SO_3)_3$ was respectively added to DME solvent to obtain 10 mmol $BiCl_3$/DME solution and 4 mmol $Bi(CF_3SO_3)_3$/DME solution. Mg foils were absolutely polished to wipe off the oxide layer and then punched into disks with a diameter of 12 mm. 60 μL $BiCl_3$/DME solution and $Bi(CF_3SO_3)_3$/DME solution was dropped on polished Mg foil. then, the reaction between solution and Mg anode surface was sustained until DME was completely volatilized at room temperature, which obtained pretreated Mg metal anode with the black surface. The pretreatment process of Mg foil using two kinds of Bi salt solutions takes about 10 minutes.

1.3 Characterizations

Field emission scanning electron microscopy (FESEM, JSM-6700F, Japan) was employed to study the micro-structure of the electrode before and after cycling. Qualitative Analysis of Elements on the Surface of Samples by XPS-Thermo ESCALAB 250XI. Ar-sputtering on very rough electrodes is not particularly useful due to the angle at which only average values are retrieved giving more or less similar spectra for a broad thickness. The element spectra of energy dispersive spectrometer (EDS) were carried out on the Oxford Inca EDS detector on Tecnai 2100. We analyzed the distribution and content of the element in Bi-based protection layer by EDS mapping, including Bi, Mg, Cl in the $BiCl_3$@Mg protection layer and Bi, Mg, S, F in the $Bi(CF_3SO_3)$@Mg protection layer.

1.4 Electrochemical performances

All cells are assembled in an Ar atmosphere glove box with the concentration of oxygen and water below 0.5 ppm. For the asymmetrical Mg//Cu cells. The electrochemical performances of modified Mg anode and pure Mg anode were examined by using CR−2032 coin-type cells with Cu foil cathode and a glass fiber separator and APC electrolyte. On the other hand, the

cathode change into Mo_6S_8 with the stainless current collector at full cell. When using a glass fiber separator, it is easy to adhere the electrode because of its rough surface. This is not conducive to our observation of the surface morphology of the electrode after 10 cycles. The polyimide (PI) film was added between the glass fiber separator and Mg anode to eliminate this handicap in the cells that were disassembled to observe the morphology of anodes after 10 cycles.

The Land CT2001A battery test system was used to test the electrochemical performance of the battery. The galvanostatic charge-discharge tests of the asymmetrical Mg//Cu cells were conducted with cut-off discharge time of 1.0 hour and the cut-off charging voltage to 1.0 V vs. Mg/Mg^{2+} at varied current densities. The rate tests were conducted at the current densities of 0.1, 0.5, 1.0, 2.0, 5.0 mA cm^{-2}, which the current density changed every five cycles. The cycling performance and coulombic efficiency of all full cells were examined with cut-off discharging voltage of 0.4 V vs. Mg/Mg^{2+} and the cut-off charging voltage to 2.0 V vs. Mg/Mg^{2+}at the current density of 1.0 C.

1.5 Computational methods

We have employed the Vienna ab initio package (VASP)[1,2] to perform all Spin-polarization density functional theory (DFT) calculations within the generalized gradient approximation (GGA) using the Perdew-Burke-Ernzerhof (PBE)[3] formulation. We have chosen the projected augmented wave (PAW) potentials[4,5] to describe the ionic cores and take valence electrons into account using a plane wave basis set with a kinetic energy cutoff of 450eV. Partial occupancies of the Kohn−Sham orbitals were allowed using the Gaussian smearing method and a width of 0.02 eV. The electronic energy was considered self-consistent when the energy change was smaller than 10^{-6} eV. A geometry optimization was considered convergent when the energy change was smaller than 0.03 eV $Å^{-1}$. Grimme's DFT-D3 methodology[6] was used to describe the dispersion interactions among all the atoms in adsorption models. What's more, Mg ions migration barrier energies had been evaluated using the climbing nudged elastic band (CI-NEB) methods. Two crystal faces of (012) and (2−22) were selected, which corresponded to the close packed planes of Bi and Bi_4O_7. More specifically, the adsorption ability towards Mg atoms on the three adsorption sites were examined.

2. Figures

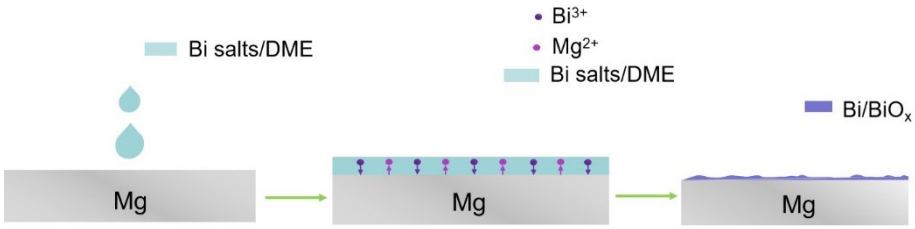

Fig. S1 Schematic illustration of pretreatment process of Mg foil.

$$BiCl_3 + Mg \rightarrow Bi + MgCl_2 \quad \textbf{(Equation S1)}$$

$$Bi(CF_3SO_3)_3 + Mg \rightarrow Bi + Mg(CF_3SO_3)_2 \quad \textbf{(Equation S2)}$$

Based on a facile redox reaction (Equation S1 and Equation S2), the metallic Mg foil and the Bi^{3+}-containing solution undergo the displacement reaction, which generates metallic Bi and Mg^{2+}. It is easily assumed that the naked Mg^{2+} transforms into solvated Mg-ions with more thermodynamical stability in DME solutions.

Previous work (ACS Appl. Mater. Interfaces 2020, 12, 25, 28298–28305) demonstrated a thick three-dimensional Bi–Mg alloy architecture by galvanic displacement reactions between $BiCl_3$/DME and the Mg metal anode combined with a post-magnesiation process. However, the thick host might badly affect the specific capacity of the Mg anode, lowering the full cell energy density.

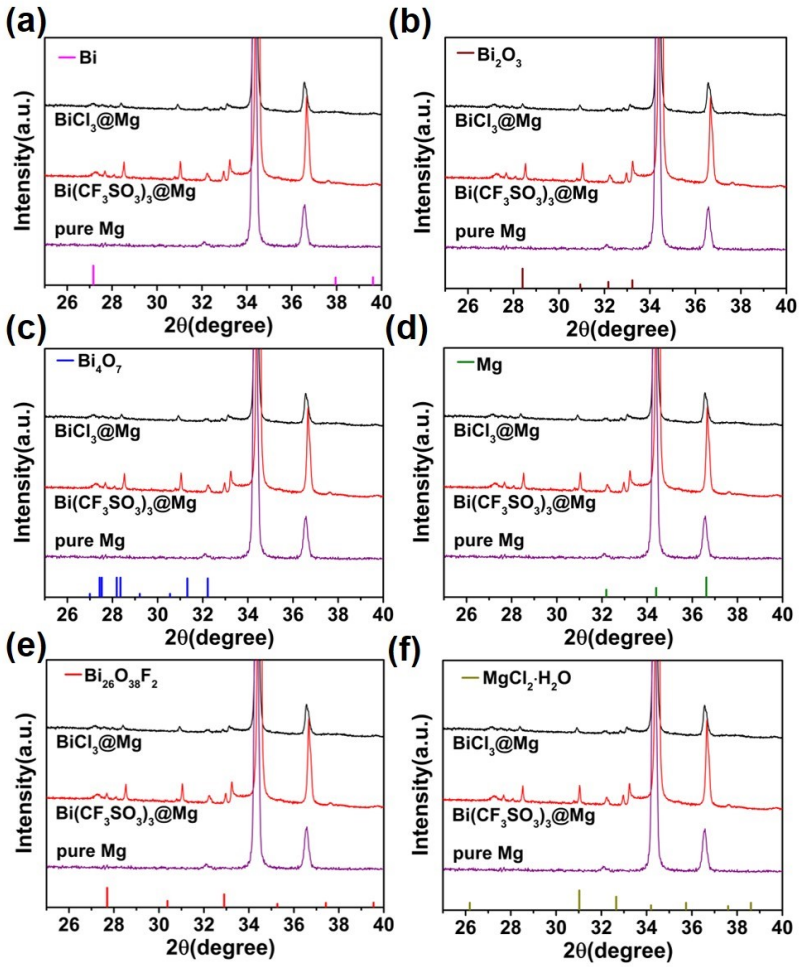

Fig. S2: XRD patterns of the $Bi(CF_3SO_3)_3$@Mg and $BiCl_3$@Mg anodes and corresponding PDF card. (a) Bi, (b) Bi_2O_3, (c) Bi_4O_7, (d) Mg, (e) $Bi_{26}O_{38}F_2$, (f) $MgCl_2 \cdot H_2O$.

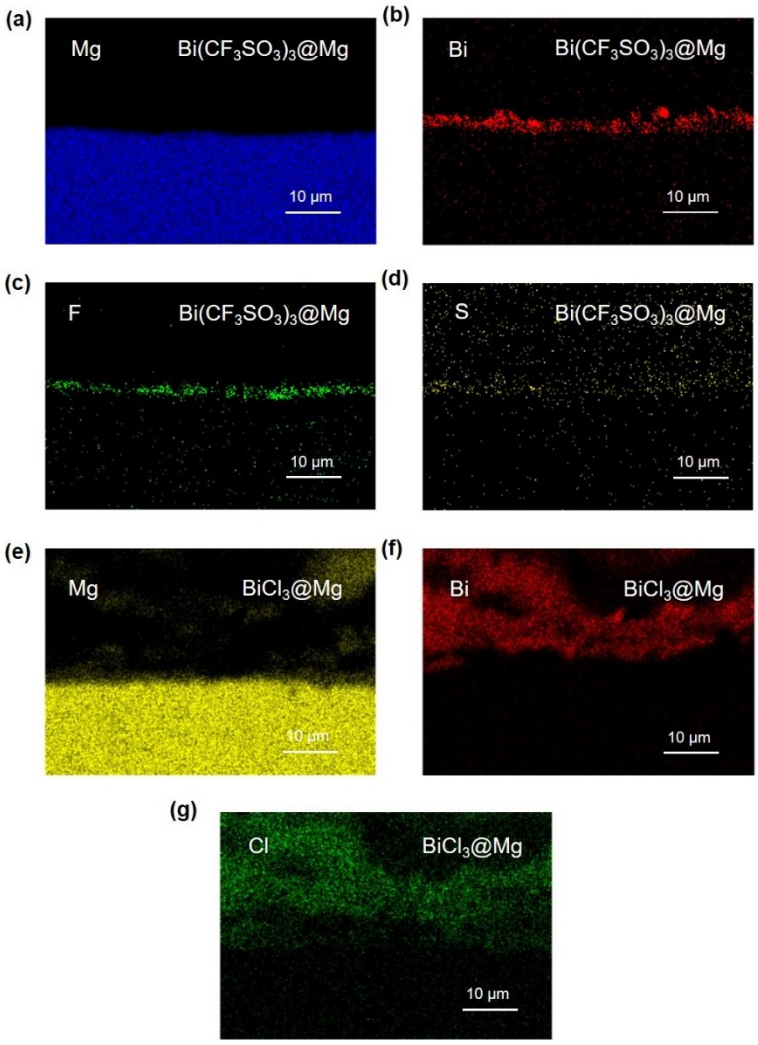

Fig. S3 EDS mapping of the Bi-based protection layers of (a-d) $BiCl_3$@Mg anode and (e-h) $Bi(CF_3SO_3)_3$@Mg anode.

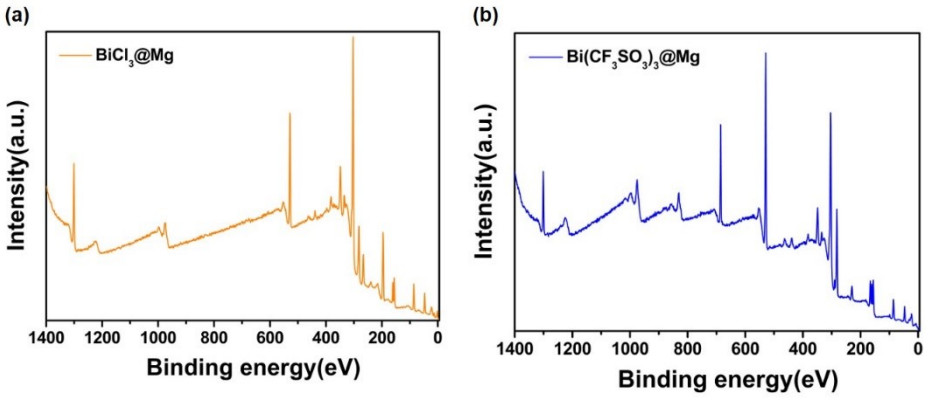

Fig. S4 The XPS full spectra of (a)$BiCl_3$@Mg anode and (b) $Bi(CF_3SO_3)_3$@Mg anode surface.

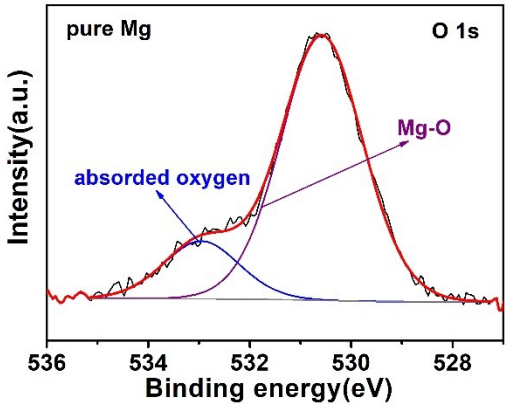

Fig. S5 XPS analysis of O 1s on the surface of pure Mg metal anodes.

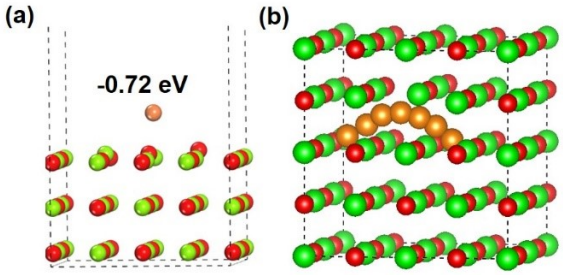

Fig. S6 The illustration of absorption site and adsorption energy of (a) MgO (1 0 0) O top for Mg ion. The migration path of Mg ion in (b) MgO

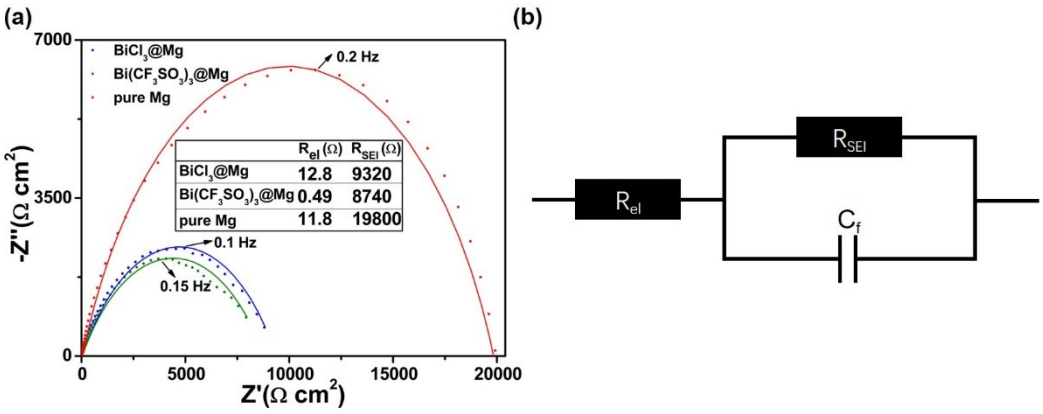

Fig. S7 (a) Electrochemical impedance spectra with fitting curve of $Bi(CF_3SO_3)_3$@Mg//Mg, $BiCl_3$@Mg//Mg and Mg//Mg cells, where R_{SEI} is SEI resistance . (b) Equivalent circuit used to calculate the value of fitting capacitance.

EIS (Electrochemical Impedance spectroscopy) measure shows that Bi-based artificial layers have lower impedance, which is in line with the result of DFT (Fig. S7a), where SEI resistances (R_{SEI}) are 8740 Ω, 9320 Ω and 19800 Ω, the resistances of the liquid electrolyte (R_{el}) are 0.49 Ω, 12.8 Ω, and 11.8 Ω for the symmetric $Bi(CF_3SO_3)_3$@Mg//Mg, $BiCl_3$@Mg//Mg and Mg//Mg cells, respectively. According to Jelena' report (Energy Technology, 2021, 9, 2001056), the contribution of liquid electrolyte in porous artificial layer to ionic conductivity could be determined by the diffusion length (L_d) and the SEI thickness (L_s). The EIS (electrochemical Impedance spectroscopy) measurements indicate that maximum frequencies (f_{max}) of the corresponding arc are varied for these symmetric cells, which are 0.15 Hz, 0.1 Hz and 0.2 Hz for the symmetric $Bi(CF_3SO_3)_3$@Mg//Mg, $BiCl_3$@Mg//Mg and Mg//Mg cells, respectively. Based on following equation, the diffusion length (L_d) could be easily determined as shown in Table S2, where ε is static dielectric constant (≈10 for SEI), ε_0 is the vacuum permittivity (≈8.854187817 × 10^{-12} F/m).

$$L_d = \sqrt{\frac{D_e}{f_{max}}} \qquad \textbf{(Equation S3)}$$

In addition, the SEI thickness (L_s) could also be determined by the following equation based on the fitting capacitance (C_f) from the constant phase element, where S is geometrical electrode

area (=1.13 cm^{-2}).

$$L_s = \frac{\varepsilon \varepsilon_0 S}{C_f} \quad \textbf{(Equation S4)}$$

Based on the value of L_d and L_s, it is assumed that the Mg-ions transport in these artificial layers is greatly beneficial from the possibly filling liquid electrolyte in porous artificial layer.

Table S1. Maximum frequencies (f_{max}), Diffusion length (L_d), Fitting capacitance (C_f) and SEI thicknesses (L_s) of $Bi(CF_3SO_3)_3$@Mg//Mg, $BiCl_3$@Mg//Mg and Mg//Mg cells.

	f_{max} (Hz)	L_d (m)	C_f (μF)	L_s (m)
$Bi(CF_3SO_3)_3$@Mg//Mg	0.15	8.2×10^{-5}	142	7.0×10^{-7}
$BiCl_3$@Mg//Mg	0.1	1×10^{-4}	145	6.9×10^{-7}
Mg//Mg	0.2	7.1×10^{-5}	30.8	3.2×10^{-6}

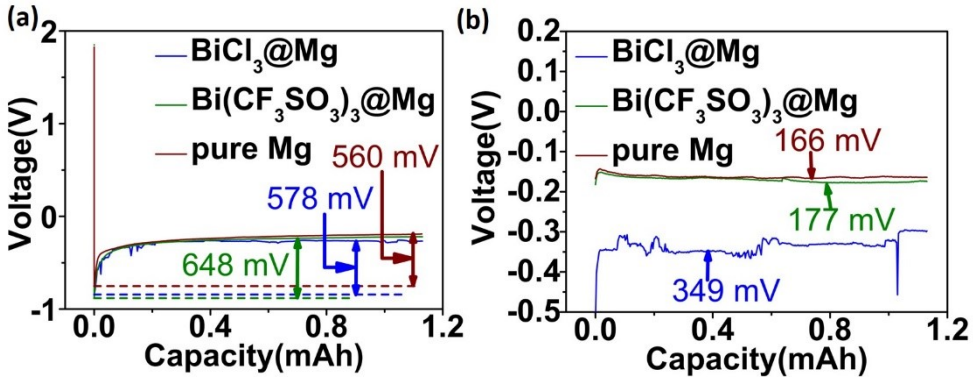

Fig. S8 Electrochemical Mg plating/stripping curve of all anodes placed in air for 2 hours at 1.0 mA cm^{-2} in (a) the first cycle and (b) second cycle.

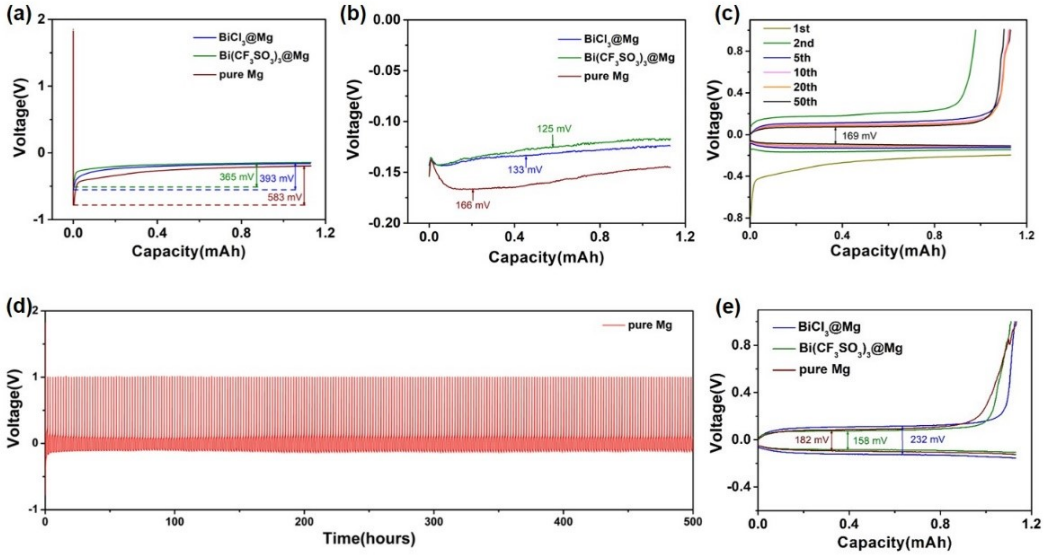

Fig. S9 Electrochemical Mg plating/stripping curve of all anodes at 1mA cm^{-2} in (a) the first cycle and (b) second cycle. (c) Galvanostatic voltage profiles of 1, 2, 5, 10, 20, 50 cycle in Mg//Cu cell at 1mA cm^{-2} and (d) voltage profiles in Mg//Cu cell at 1mA cm^{-2}. (e) Galvanostatic voltage profiles of 250 cycle in pretreated-Mg//Cu cell and pure Mg//Cu cell at 1mA cm^{-2}.

The relatively low nucleation and plateau overpotentials might be ascribed to the magnesiophilic ability and the fast Mg atom migration kinetics of the Bi-based species in the artificial interphases. The above results verify that the Bi-containing artificial layers reduce the nucleation and deposition barriers in line with theoretical expectations, while BiO_x/MgO might hinder the adsorption and transport of Mg.

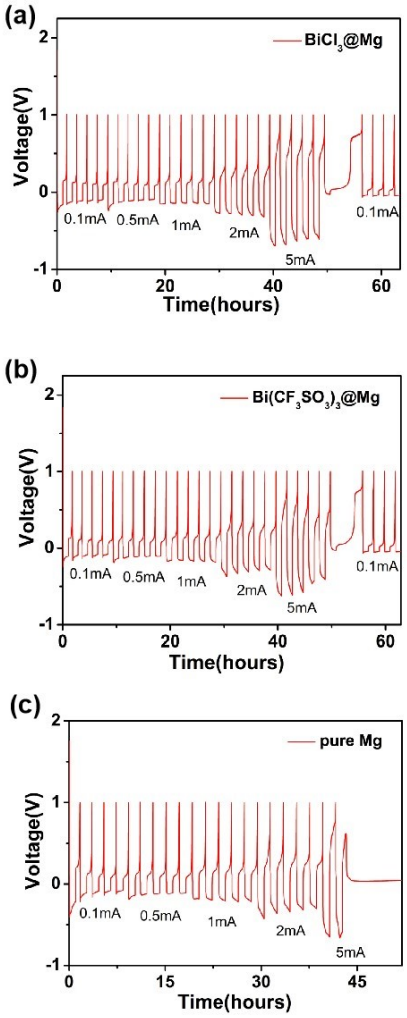

Fig. S10 The rate performance of (a) the $BiCl_3$@Mg//Cu cell, (b) the $Bi(CF_3SO_3)_3$@Mg//Cu cell and (c) the pure Mg//Cu cell.

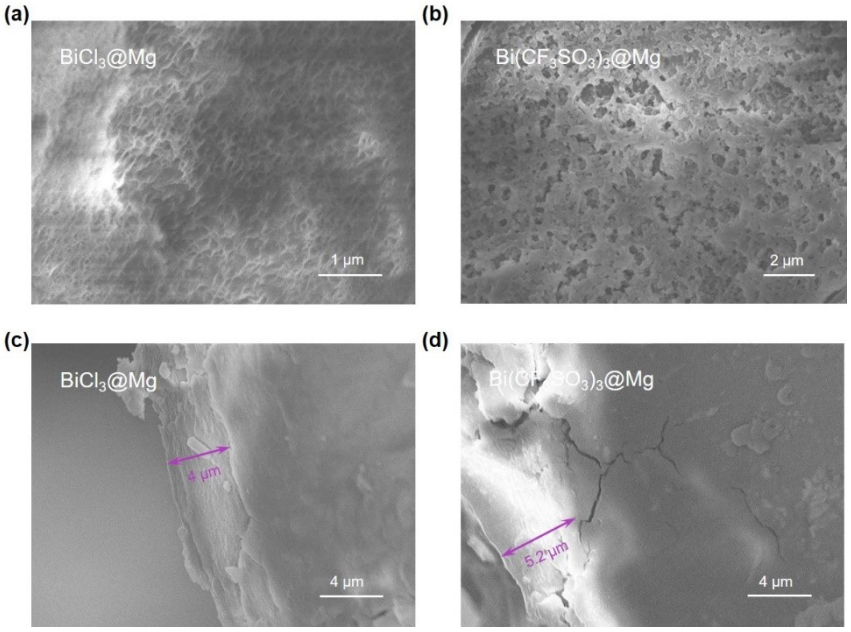

Fig. S11 Top-view (a and b) and cross-sectional (c and d) SEM images of the $BiCl_3$@Mg (a and c) and $Bi(CF_3SO_3)_3$@Mg (b and d) anodes after 10 cycles.

Both the surface and cross-sectional SEM images were investigated to elucidate the cycle stability. Porous structure was disclosed for the $BiCl_3$@Mg and $Bi(CF_3SO_3)_3$@Mg anodes as shown in surface SEM images (Fig. S11a−b). This was speculated to provide numerous nucleation spots and shorten the pathway of Mg-ions. The cross-sectional SEM images demonstrated that the artificial interphase still existed. Their thicknesses are detected to be 4 μm and 5.2 μm for the $BiCl_3$-based and $Bi(CF_3SO_3)_3$-based artificial interphases (Fig. S11c−d), respectively. This result illustrated that the artificial interphase could not dissolve in all phenyl complex (APC) electrolyte.

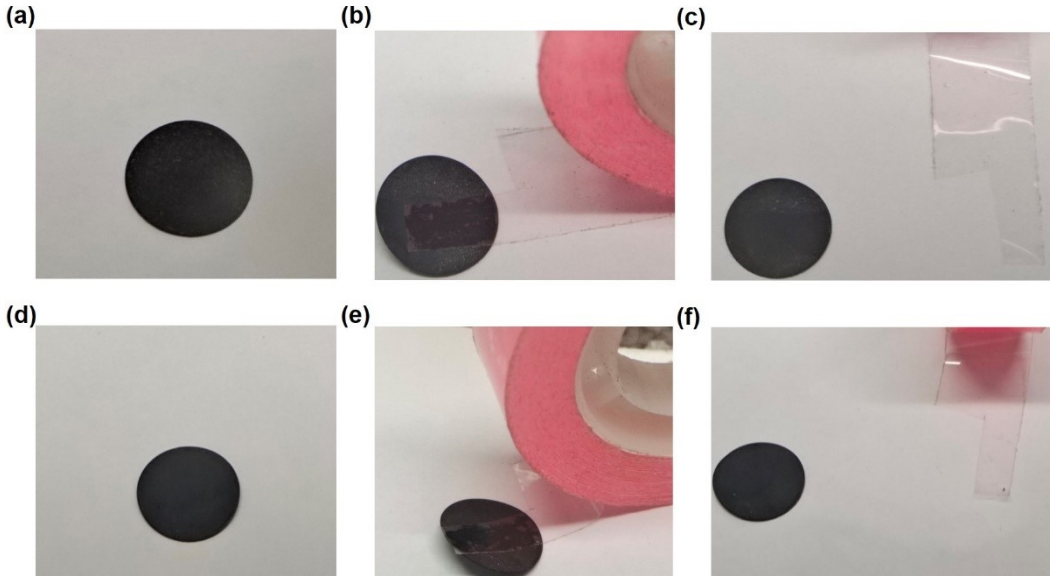

Fig. S12 The facile tape tearing experiment of $BiCl_3$@Mg anode (a, b: before tearing; c: after tearing). The facile tape tearing experiment of $Bi(CF_3SO_3)_3$@Mg anode (d, e: before tearing; f: after tearing).

The Bi-containing artificial layer was assumed to not form a strong chemical bond with Mg foil given that metallic Mg shall reaction with Bi to form Bi-Mg alloys (ACS Appl. Mater. Interfaces 2020, 12, 25, 28298–28305; ACS Energy Lett. 2021, 6, 2594−2601). However, to accurately determine the interaction between Bi-containing artificial layer and Mg foil is not a trivial. The cohesive strength of the Bi-containing artificial layer on the Mg foil was evaluated by the facile tape tearing experiment. It could be noted that the tape cannot easily peel the Bi-based artificial layers from the Mg foil, indicating that there is a strong bond between the protective layers and the substrate.

.

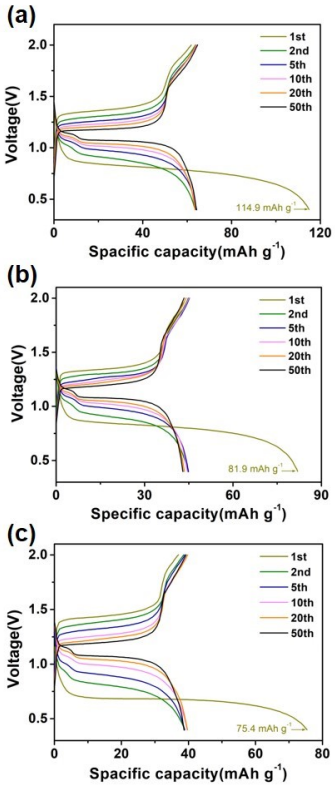

Fig. S13 Typical charge/discharge profiles of (a) the $BiCl_3$@Mg//Mo_6S_8 cell, (b) the $Bi(CF_3SO_3)_3$@Mg//Mo_6S_8 cell and (c) the pure Mg//Mo_6S_8 cell at 1 C.

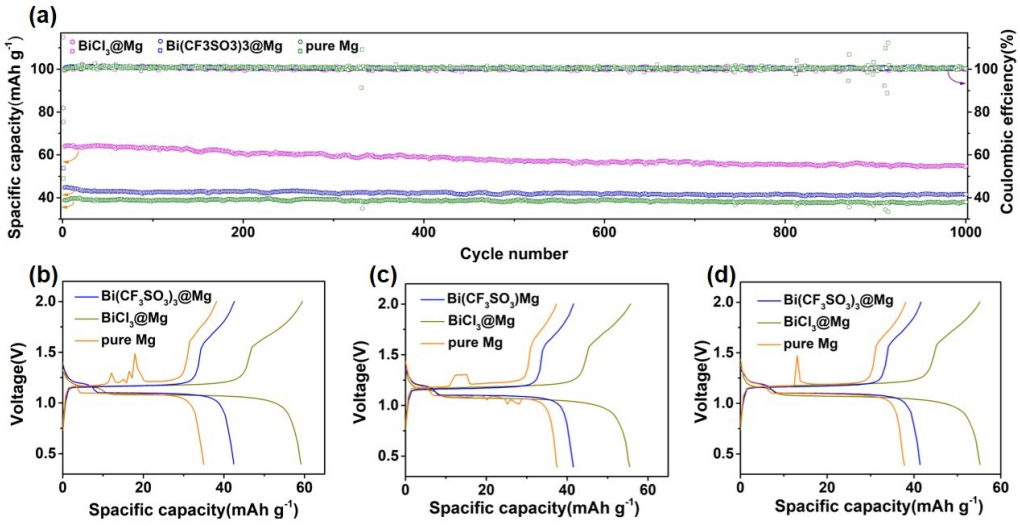

Fig. S14 (a) Discharge capacities vs. cycle numbers of the pretreated-Mg//Mo_6S_8 cell and pure Mg//Mo_6S_8 cell. Typical charge/discharge profiles of the pretreated-Mg//Mo_6S_8 cell and the pure Mg//Mo_6S_8 cell at (b) 333, (c) 812, (d) 913 cycle at 1 C.

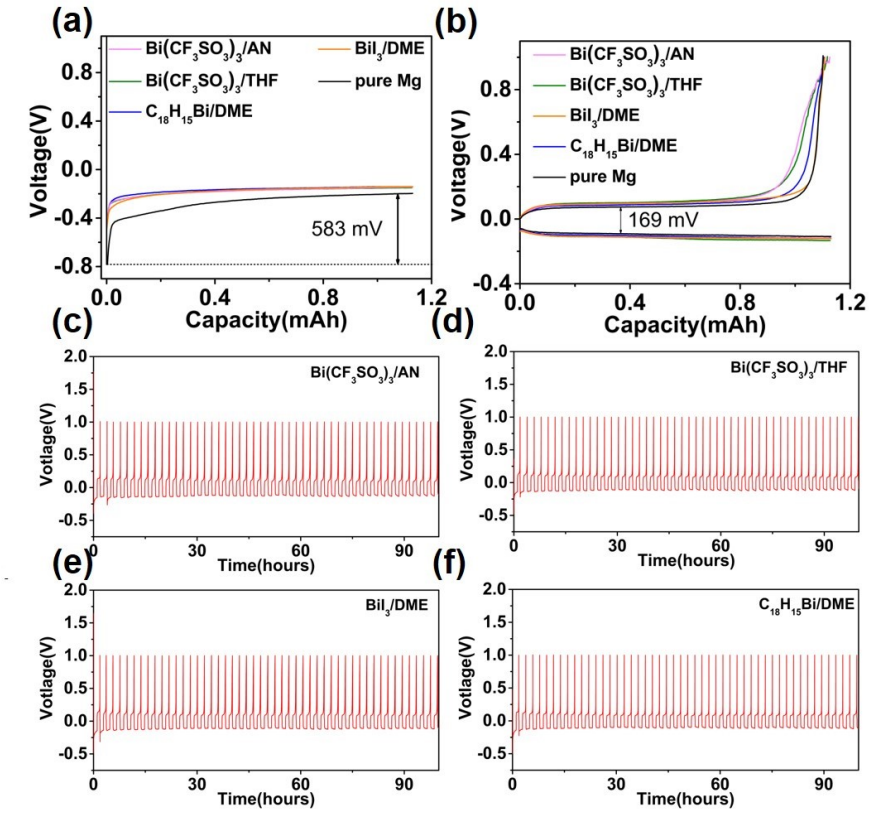

Fig. S15 Electrochemical Mg plating/stripping curve of anodes pretreated with different solutions at 1 mA cm^{-2} in (a) the first cycle and (b) 50th cycle. (c)-(f) Galvanostatic voltage profiles of anodes pretreated with different solutions at 1 mA cm^{-2}.

We have tested the effects of other Bi salts and different solvents. It is found that the Bi salts-treated Mg foils, namely the bismuth iodide (BiI_3) and triphenyl bismuth (TPB) display lower nucleation overpotential during Mg electrodeposition (Fig. S13 and Table S2), demonstrating its feasibility and reliability as potential modifiers. Besides, the solution of $Bi(CF_3SO_3)_3$ in THF and AN can also decrease the nucleation overpotential during Mg electrodeposition. However, it is also worth noting that these above protective layers modified by the above solutions (with BiI_3, TPB, in DME or $Bi(CF_3SO_3)_3$ in THF and AN) deliver much larger voltage polarization during the dynamic Mg growth processes (voltage plateaus region). Moreover, $BiCl_3$ cannot be dissolved in AN and THF. Considering the above factors, the $BiCl_3$/DME and $Bi(CF_3SO_3)_3$/DME solutions have been chosen to pretreat the Mg foil in this work.

Table S2 Nucleation overpotentials and polarization voltages of Mg foil pretreated with different solutions.

Pretreatment solution	Nucleation overpotential (mV) at 1 mA cm^{-2}	Polarization voltage (mV) at 50^{th} cycle
$BiCl_3$/DME	393	146
$Bi(CF_3SO_3)_3$/DME	365	167
$Bi(CF_3SO_3)_3$/AN	244	212
$Bi(CF_3SO_3)_3$/THF	337	182
BiI_3/DME	343	201
$C_{18}H_{15}Bi$/DME	356	198
Pristine Mg	583	169

References:

1 G. Kresse and J. Furthmüller, *Comput. Mater. Sci.*, 1996, **6**, 15-50.

2 G. Kresse and J. Furthmüller, *Phys. Rev. B*, 1996, **54**, 11169.

3 J. P. Perdew, K. Burke and M. Ernzerhof, *Phys. Rev. Lett.*, 1996, **77**, 3865.

4 G. Kresse and D. Joubert, *Phys. Rev. B*, 1999, **59**, 1758.

5 P. E. Blöchl, *Phys. Rev. B*, 1994, **50**, 17953.

6 S. Grimme, J. Antony, S. Ehrlich and H. Krieg, *J. Chem. Phys.*, 2010, **132**, 154104.